npj | microgravity

www.nature.com/npjmgrav

ARTICLE OPEN

Rotation related systematic effects in a cold atom interferometer onboard a Nadir pointing satellite

Quentin Beaufils[1]✉, Julien Lefebve[2], Joel Gomes Baptista[1], Raphaël Piccon[1], Valentin Cambier[1], Leonid A. Sidorenkov[1], Christine Fallet[2], Thomas Lévèque[2], Sébastien Merlet[1] and Franck Pereira Dos Santos[1]

We study the effects of rotations on a cold atom accelerometer onboard a Nadir pointing satellite. A simulation of the satellite attitude combined with a calculation of the phase of the cold atom interferometer allow us to evaluate the noise and bias induced by rotations. In particular, we evaluate the effects associated to the active compensation of the rotation due to Nadir pointing. This study was realized in the context of the preliminary study phase of the CARIOQA Quantum Pathfinder Mission.

npj Microgravity (2023)9:53 ; https://doi.org/10.1038/s41526-023-00297-w

INTRODUCTION

Quantum inertial sensors based on cold atom interferometry have reached a level of performances and maturity allowing for scientific and commercial use in various ground based applications[1]. Their sensitivity and accuracy are expected to increase dramatically in microgravity, where the interrogation time is no longer limited by the size of the instrument[2,3]. This triggered a recent interest in developing this technology for space[4–6] with potential applications in geodesy[7–11], fundamental physics[12,13], navigation and gravitational wave observation[14,15]. Opening the way to those developments, the CARIOQA Pathfinder Mission[16] aims at realizing the first quantum accelerometer on a satellite. This space mission will consist in a single axis cold atom accelerometer designed to measure the non-gravitational acceleration along the velocity direction of a satellite on low Earth orbit. The mission is meant to realize key milestones for space atom interferometry and demonstrate unprecedented performances for quantum accelerometers.

Adapting cold atom accelerometers to low orbit environment requires to take into account residual fluctuating rotation of the satellite due to atmospheric and solar winds. Besides, various future missions (including CARIOQA) will require to operate in a Nadir pointing orbit, which implies a constant angular velocity in the mrad/s range. It has been identified[17] that this rotation must be compensated to avoid a dramatic loss of contrast due to inhomogeneous Coriolis effect. In this article, we study the impact of rotation on the sensitivity and accuracy of the future CARIOQA cold atom accelerometer. We evaluate the phase of a rotating atom interferometer, with and without compensation, and identify a systematic effect related to rotation compensation. This systematic effect is then demonstrated experimentally. We realize a simulation of the attitude of a low orbit satellite to obtain angular velocity time series and we use those time series to estimate the noise associated to residual rotation fluctuations and to the rotation compensation system.

RESULTS AND DISCUSSION

Evaluation of the phase of a rotating atom interferometer

The system considered is a single axis Mach–Zehnder-like Chu Bordé cold atom interferometer[18–20] embarked in a Nadir pointing satellite. The interferometer's measurement axis is aligned with the velocity vector axis (*x*-axis). A mirror (M) used to retro-reflect the interferometer laser beams is rigidly fixed to the case of the satellite and constitutes the reference against which the acceleration of the free falling atom cloud (A) is measured. In this configuration, the instrument measures the non gravitational acceleration of the satellite along the *x*-axis. All positions are defined relative to the center of mass of the satellite O which is taken as the origin of a reference frame aligned with the satellite main axes (see Fig. 1).

We evaluate the output phase of the interferometer in the presence of an acceleration along *x* and a small angular velocity $\mathbf{\Omega}(t) = (\Omega_x(t), \Omega_y(t), \Omega_z(t))$ on O ($\Omega T \ll 1$ where T is the time between two interferometer's pulses, and $2T$ is the total duration of the interferometer). The configuration considered is a three pulses Raman interferometer with double diffraction[21]. The total output phase difference can be expressed as a sum of the laser interaction phases during the interferometer:

$$\Delta\phi = 2\phi_1 - 2\phi_{A2} - 2\phi_{B2} + \phi_{A3} + \phi_{B3}, \quad (1)$$

where the letters label the two paths of the interferometer and the numbers the three successive pulses.

The effective laser wave vector $\mathbf{k}_{\text{eff}}$ is defined by the orientation of the retroreflection mirror M. When the mirror is fixed in the satellite frame, $\mathbf{k}_{\text{eff}}$ is constant and we can write:

$$\Delta\phi = 2\mathbf{k}_{\text{eff}} \cdot [\mathbf{r}_0 - 2(\mathbf{r}_A(T) + \mathbf{r}_B(T)) + (\mathbf{r}_A(2T) + \mathbf{r}_B(2T))], \quad (2)$$

where $\mathbf{r}_A(t)$ (resp. $\mathbf{r}_B(t)$) is the classical position of the atomic wave packet on the path A (respectively B) of the interferometer at time t.

We evaluate the classical trajectory of the atoms in the non Galilean satellite reference frame by solving the equations of motion using a polynomial ansatz with the Lagrangian:

$$L = \frac{1}{2}m(\dot{\mathbf{r}} + \mathbf{\Omega} \times \mathbf{r})^2 + m\mathbf{a} \cdot \mathbf{r} \quad (3)$$

where $\mathbf{a}$ is the linear acceleration of the atoms relative to the satellite case, which corresponds to the non-gravitational acceleration of the satellite, and m is the atomic mass.

[1]LNE–SYRTE, Observatoire de Paris, Université PSL, CNRS:UMR 8630, Sorbonne Université, 61 avenue de l'Observatoire, F–75014 Paris, France. [2]Centre National d'Etudes Spatiales, 18 avenue Edouard Belin, 31400 Toulouse, France. ✉email: quentin.beaufils@obspm.fr

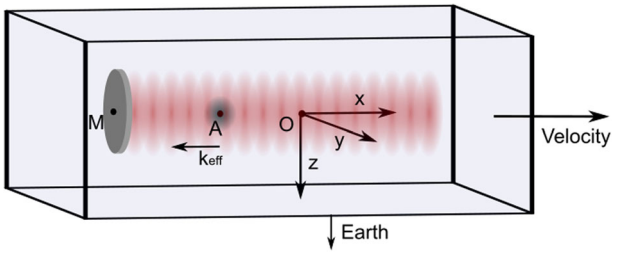

Fig. 1 The interferometer geometry in the satellite. The reference frame used in this work has the satellite center of mass O as origin, the flight vector axis as *x*, the cross track axis, perpendicular to orbital plane, as *y*, and the Nadir axis as *z*. The atom cloud's mean position is A and the mirror's position is M.

Atomic wave packet positions are evaluated at each pulse and inserted in equation (1). We obtain to second order in ΩT:

$$\Delta\phi = 2k_{\text{eff}}T^2\left[a_x + G_{xx}x_0 + G_{xy}y_0 + G_{xz}z_0\right. \tag{4}$$

$$+2v_{z0}\Omega_y + 2v_{y0}\Omega_z \tag{5}$$

$$\left.+z_0\Omega_x\Omega_z - x_0\left(\Omega_z^2 + \Omega_y^2\right) + y_0\Omega_y\Omega_x\right], \tag{6}$$

where $\mathbf{r}_0 = (x_0, y_0, z_0)$ is the initial position of the atoms and (v_{x0}, v_{y0}, v_{z0}) their initial velocity in the satellite frame and $\mathbf{G}_x = (G_{xx}, G_{xy}, G_{xz})$ is the gradient of the component along *x* of the Earth's gravity. Here $\mathbf{\Omega} = (\Omega_x, \Omega_y, \Omega_z)$ is the temporal mean of the time dependant angular velocity during the interferometer. Besides acceleration along the *x*-axis, this expression shows that the interferometer is sensitive to Coriolis (term 5) and centrifugal accelerations (term 6). In the context considered in this article, rotation rates are always smaller or on the order of 10^{-3} rad/s. As a consequence, the higher order terms are at least 3 orders of magnitude smaller than the terms in the above equation and will be ignored. For example, third order terms corresponding to the interplay between the gravity gradient and rotations (i.e. $T\Omega_y G_{xx} z_0$) are on the order on 10^{-15} m s^{-2}.

In Nadir pointing navigation at the considered altitude, the satellite has a mean angular velocity of $\Omega_N \simeq 1$ mrad/s around the *y*-axis. Given the initial velocity spread of the atoms, Coriolis acceleration is expected to induce a phase inhomogeneity across the cloud and limit the instrument[17]. Even at a temperature as low as $T_e \simeq 100$ pK, the interferometer contrast would drop drastically for interrogation times *T* larger than 1 s. The commonly accepted solution is to compensate the Nadir rotation by counter-rotating the retro-reflection mirror at the same rate during the interferometer[22,23]. The effective wave vector $\mathbf{k}_{\text{eff}}$ has then a fixed direction in the inertial frame but varies in the satellite frame. In this case equation (2) is no longer valid.

To take into account the variation of $\mathbf{k}_{\text{eff}}$ in the satellite frame during a rotation compensated interferometer sequence, we define $\mathbf{\Omega}_M = (0, \Omega_M, 0)$ as the constant angular velocity of the mirror, and $\mathbf{r}_M = (x_M, y_M, z_M)$ the position of its center of rotation. We also consider the possibility to rotate the incoming laser beam and define its angular velocity $\mathbf{\Omega}_I = (0, \Omega_I, 0)$. A geometrical calculation of the laser phase at position $\mathbf{r} = (x, y, z)$ as a function of the mirror and incoming beam orientation yields

$$\phi(\mathbf{r}, \mathbf{r}_M, \theta_I, \theta_M) = k_{\text{eff}}\cos(\theta_I - \theta_M)[(x_M - x)\cos(\theta_M) - (z_M + z)\sin(\theta_M) - d_M], \tag{7}$$

where we define d_M as the distance between the mirror's reflection plane and its center of rotation M. θ_M (respectively θ_I) is the angle between the mirror's reflection plane (resp. the incoming beam's equiphase plane) and the *z*-axis (see Fig. 2). For the following, both angles are linked to angular velocities by the

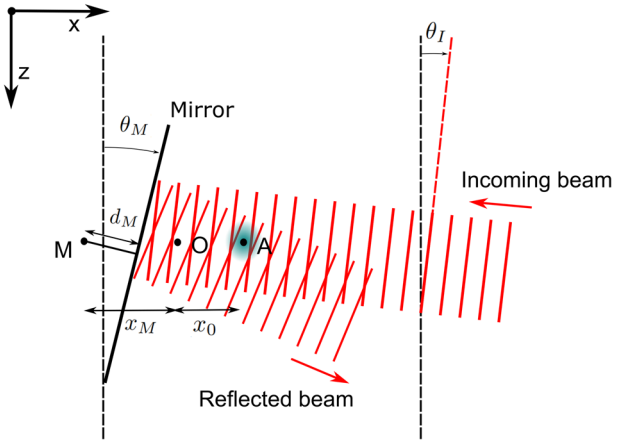

Fig. 2 Outline of the geometrical configuration of the rotation compensated atom interferometer. The atomic cloud (A) is interrogated by a Raman beam with incoming angle θ_I, reflected on a mirror rotating around the point M, and forming an angle θ_M with the *z*-axis.

relations:

$$\begin{aligned}\theta_i(t=0) &= -\Omega_i T\\ \theta_i(T) &= 0\\ \theta_i(2T) &= \Omega_i T,\end{aligned} \tag{8}$$

where *i* stands for M and I.

Using expression (7) in the semi-classical description detailed in the section "Introduction", we obtain

$$\Delta\phi = 2k_{\text{eff}}T^2\left[a_x + G_{xx}x_0 + G_{xy}y_0 + G_{xz}z_0\right. \tag{9}$$

$$+2v_{z0}(\Omega_y + \Omega_M) + 2v_{y0}\Omega_z$$

$$+z_0\Omega_x\Omega_z - x_0(\Omega_z^2 + \Omega_y^2) + y_0\Omega_y\Omega_x \tag{10}$$

$$\left.+(x_0 - x_M)(\Omega_M^2 + (\Omega_M - \Omega_I)^2)\right]. \tag{11}$$

As expected, the Coriolis acceleration due to Ω_y vanishes for $\Omega_M = -\Omega_y$. Besides, a term (11) corresponding to the motion of the mirror in the satellite appears in the phase expression. The centrifugal acceleration due to Nadir rotation around *y*-axis is compensated only when this term is equal to $x_0\Omega_y^2$, which requires $\Omega_M = \Omega_I = -\Omega_y$, but also $x_M = 0$. This corresponds to the situation when the mirror's rotation axis is aligned with the satellite's inertial center, which is the only situation when the mirror's reflection plane does not move in the inertial frame.

We observed experimentally this phase term (11) using a ground based cold atom gravity gradiometer. The experimental setup, described in[24], consists in two cold atom clouds in free fall, vertically separated by a distance $d = 1$ m, and interrogated by the same pair of counter-propagating Bragg laser beams. The common reference mirror is mounted on a tip-tilt platform and can be rotated with a controlled constant angular velocity Ω_M during the interferometer sequence. The incoming laser beam was fixed ($\Omega_I = 0$), and for a differential measurement the rotation compensation phase can be expressed as:

$$\Delta\phi_{RC}/(k_{\text{eff}}T^2) = 2d\Omega_M^2.$$

Here we use single diffraction Bragg pulses, which explains a phase smaller by a factor of 2 compared to the calculation for double diffraction. In order to probe this result, we performed a differential phase measurement of the two interferometers of duration $T = 10$ ms as a function of the angular velocity. The differential phase at $\Omega_M = 0$ was taken as a zero reference point in

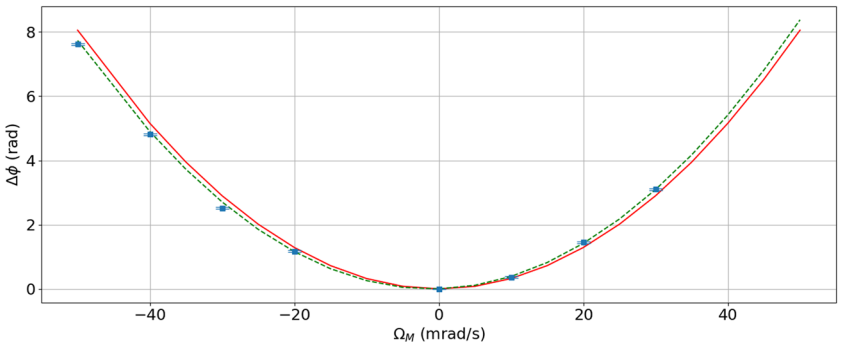

Fig. 3 Differential phase of the vertical gravity gradiometer, as a function of the reference mirror's angular velocity during the measurement. Red solid line: quadratic term $\Delta\phi_{RC} = 4k_{\mathrm{eff}}T^2 d\Omega_{\mathrm{M}}^2$. Green dashed line: fit of the data with $f(\Omega_{\mathrm{M}}) = 2k_{\mathrm{eff}}T^2(d\Omega_{\mathrm{M}}^2 + \delta v_0\Omega_{\mathrm{M}})$.

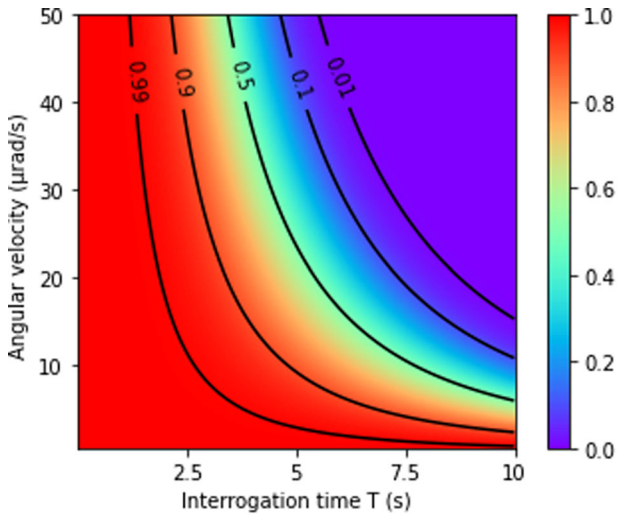

Fig. 4 Effect of the inhomogeneous Coriolis acceleration. Inhomogeneous Coriolis acceleration limited contrast of the interferometer as a function of the total angular velocity and interrogation time, for an atomic effective temperature of $\Theta = 4 \times 10^{-11}$ K.

order to extract the angular velocity dependence only. The measurement is displayed in Fig. 3 and compared to theory without adjusted parameters (red solid line). We observed a small discrepancy, that can be explained by the presence of a residual differential transverse velocity δv_0 between the two clouds that causes a Coriolis effect $\Delta\phi_{\mathrm{coriolis}}/(k_{\mathrm{eff}}T^2) = 2\delta v_0\Omega_{\mathrm{M}}$. The green dashed line shows the result of a fit of the data with the sum of the quadratic and linear term, using δv_0 as the only adjustable parameter. We obtain the value $\delta v_0 = 1.3 \pm 0.11$ mm/s. Residual dispersion of the measured phase around the expected value larger than statistical uncertainty can be due to laser phase profile inhomogeneity.

The inhomogeneous Coriolis effect

The velocity spread of a finite temperature atom cloud induces a phase inhomogeneity that alters the contrast of the interferometer[17]. The CARIOQA interferometer will rely on a delta kick collimated atom source similar to the one described in[25], which effective temperature can be lowered to $\Theta = 4 \times 10^{-11}$ K. Figure 4 shows the contrast at this temperature, as a function of the interrogation time and the angular velocity's absolute value. We observe that the contrast vanishes rapidly when T increases, unless the residual angular velocity remains close to 1 μrad/s. This can be achieved by counter rotating the reference mirror, which implies a real time knowledge of the satellite's angular velocity during the interferometer sequence to that level of stability, but also a control over the angle of the rotating mirror and incoming beam down to about a few microrad. An alternative or complementary technique, point source interferometry[23] with a spatially resolved detection, can also be used to reveal the velocity dependent phase structure in the atomic cloud. However, in this process the quantum projection noise limited sensitivity is reduced by a least a factor $\sqrt{2}$ due to fewer atoms participating to the measurement.

For the following, we consider a rotation compensation with a shot to shot standard deviation of the angular velocity of 1 μrad/s, with an angular velocity compensation perfectly aligned around the y-axis, that follows the driven orbital angular velocity from the AOCS.

Table 1. Simulation parameters.

Parameter	Value	Unit	Comment
T	1 to 5	s	Interferometer interrogation time
N	10^5		Atom number
C	0.8		Contrast
r_0	1	mm	Initial mean position of the cloud
v_0	100	μm/s	Initial mean velocity of the cloud
Θ	40	pK	Effective temperature of the cloud

The phase noise associated to residual rotation

Using the phase expression found in the section "The inhomogeneous Coriolis effect" and the attitude simulation described in the section "Methods", we estimate the phase noise associated with residual (uncompensated) rotation noise of the satellite and compare it to the expected sensitivity of a quantum projection noise (QPN) limited atom interferometer with $N = 10^5$ atom, as expected for the CARIOQA instrument. The parameters used for this comparison are given in Table 1. We use state of the art values for the interferometer, except for the interrogation time T which is the main variable parameter for the future mission. As the future performances depend strongly on T, we consider different values between 1 s and 5 s.

The Centrifugal acceleration noise depends on the initial distance between the atom cloud and the center of mass of the satellite. The control over this value is expected to be limited by the knowledge of the center of mass's position in the satellite frame, to about 1 mm. The Coriolis acceleration depends on the initial mean velocity of the atom cloud. From[25], we anticipate a delta kick collimated atom source with a residual initial mean velocity v_0 of about 100 μm/s.

The effect of time-dependent perturbations on the atom interferometer is modeled using the formalism of the sensitivity

function[26]. If we describe the rotation noise source by a power spectral density (PSD) $S(f)$, the resulting RMS phase noise of the atom interferometer is calculated as:

$$\sigma_\phi^2 = \int_0^\infty S(f)|H(f)|^2 \, \mathrm{d}f$$

where $H(f)$ is the atom interferometer transfer function. For this simulation, we also took into account a potential loss of contrast due to the inhomogeneous Coriolis acceleration.

Figure 5 shows the amplitude spectral density (ASD) of the Coriolis and centrifugal acceleration noise, as well as the expected QPN limited sensitivity of the instrument. We observe that maintaining a rotation induced phase noise level below QPN is thus possible using a state of the art atom interferometer and a commercial AOCS system.

The phase noise associated to the rotation compensation

As shown in the section "Introduction", the nadir rotation compensation induces a phase shift to the interferometer if the center of rotation of the mirror (M) is not perfectly superimposed to the center of mass (O) of the satellite. A noise associated to this phase can appear because of an imperfect control of the rotating mirror's angle and limit the sensitivity of the instrument. The usually considered technical solution for rotating the mirror is to use a piezoelectric tip-tilt platform. With this technique M is usually close to the mirror, which implies a distance of a few tens of centimeters between M and the initial position of atoms A. Based on commercially available systems, we anticipate a shot to shot jitter of the mean rotation rate Ω_M of $\sigma_{\Omega_M} = 1\,\mu$ rad/s. Under those circumstances a trade off appears between minimizing this noise and the centrifugal acceleration noise mentioned in the section "The phase noise associated to residual rotation", by respectively placing the center of mass of the satellite close to M or close to A. This is illustrated by Fig. 6 where we evaluated the rotation noise limited sensitivity, defined as the total phase noise of the instrument for an equivalent 1 s measurement, as a function of the position of the atoms-mirror ensemble relatively to the center of mass ($x_0 = \mathrm{OA}$), for two different distances between the atoms and the mirror (AM). The smallest possible distance for a $t = 5$ s interrogation time is AM = 6 cm. We also compare between the situation when only the reference mirror is rotated ($\Omega_I = 0, \Omega_M = -\overline{\Omega}_y$), and both the mirror and the incoming beam are rotated ($\Omega_I = \Omega_M = -\overline{\Omega}_y$). The parameters given in Table 1 were used for this evaluation. The sensitivity is limited by centrifugal acceleration for large x_0, and by rotation compensation noise for small x_0 (large x_M).

As expected, the shorter distance AM is more favorable. Rotating the incoming beam also allows to improve the sensitivity by a factor two (see equation (11)). In the best case, we observe that the sensitivity of the instrument is limited to approximately 5×10^{-10} m.s^{-2}.Hz$^{-1/2}$, which is above QPN for an interrogation time of 5 s. A way to improve this limitation could be to use a specifically designed rotation compensation system with a custom position of the rotation center far from the mirror. This way, the rotation center of the mirror and the mean atomic position could both be superimposed to the center of mass of the satellite. This can be done by translating the tip-tilt platform during the rotation.

Besides the limitation on the sensitivity of the instrument, its accuracy and long term stability can be also limited by the rotation compensation system. The phase term associated to the rotation of the mirror and of the incoming beam can be as large as a few 10^{-7} m.s^{-2} if x_M is a few centimeters. Satellite navigation relies on rocket fuel propulsion that may cause a long term drift of

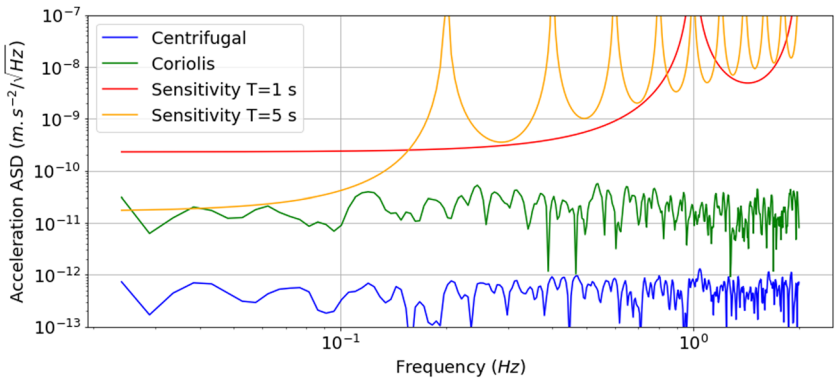

Fig. 5 Effect of the residual rotations. Amplitude spectral density of acceleration noise due to residual rotations of the satellite compared to expected QPN limited sensitivities calculated for $T = 1$ s and $T = 5$ s.

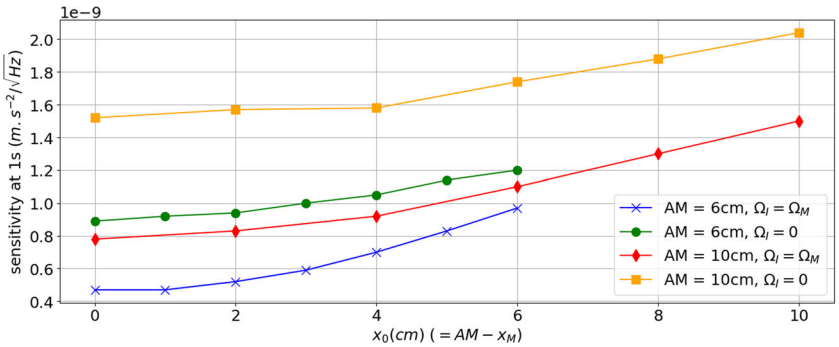

Fig. 6 Limitation of the instrument due to the rotation compensation. Sensitivity limit associated to rotation noise as a function of the position of the instrument (atoms and mirror) in the satellite, for two different distances between the atoms and the mirror's rotation center, and with or without incoming beam rotation. x_0 is the distance atoms—center of mass of the satellite.

the position of the center of mass. Under the conditions considered, the measurement bias associated to mirror rotation is on the order of 10^{-7} m. s^{-2} with a variation of 10^{-9} m. s^{-2} per millimeter drift of the position of the center of mass. A precise modeling of the center of mass variations may be necessary to evaluate this systematic effect. Alternatively, a calibration of the bias term could be performed by varying the satellite's total angular velocity.

In this article we evaluated the effect of rotations on the performances of a cold atom accelerometer in a low orbit Nadir pointing satellite for the future CARIOQA mission. A simulation of the satellite's attitude along with a calculation of the interferometer's phase allowed to specify some instrumental parameters such as the initial velocity of the atomic cloud, its positioning in the frame of the satellite and its temperature. We showed that it is possible to maintain the rotation related phase noise limit on the sensitivity of the instrument down to a few 10^{-10} m. s^{-2}. Hz$^{-1/2}$ in low orbit with a relatively standard attitude control system and state of the art ultra-cold atom technology. This was illustrated by a specific set of parameters, however future design studies may aim at better performances by either improving the AOCS or the cold atom system.

When the Nadir rotation is compensated, we identified a phase term due to an imperfect alignment between the rotation axis of the mirror and the center of mass of the satellite. This term can limit the sensitivity of the instrument, as well as its accuracy. The rotation compensation system has to be designed in accordance in the frame of the CARIOQA Quantum Pathfinder Mission, as well as in other future space atom interferometry missions.

METHODS

Simulation of the satellite attitude

We performed a Matlab/Simulink simulation of the future CARIOQA satellite attitude in order to obtain realistic angular velocity time series. Figure 7 shows a diagram of the Attitude and Orbit Control System (AOCS) mono-axial simulator (each axis was simulated independently). The perturbation torque on the satellite was computed using a complex simulator able to evaluate precise atmospheric, solar pressure, magnetic and gravity gradient torques. The actuator considered was an electric propulsion system modelized as a first order transfer function with a white noise consistent with the propulsion system used on the MICROSCOPE project[27]. We used a 4 Hz gyrostellar attitude determination system[28], composed of a star tracker consistent with the HYDRA equipement caracteristics, and a gyrometer consistent with the ASTRIX-NS. It consists in a simplified version of a gyrostellar Kalman filter with a low-pass second order filter on the star tracker measurements and a high-pass second order filter on the gyrometer measurements with the same cut-off frequency (the hybridization frequency). An estimation of the gyrometer default (bias and scale factor) was also added to the estimator part to improve the angular velocity estimation.

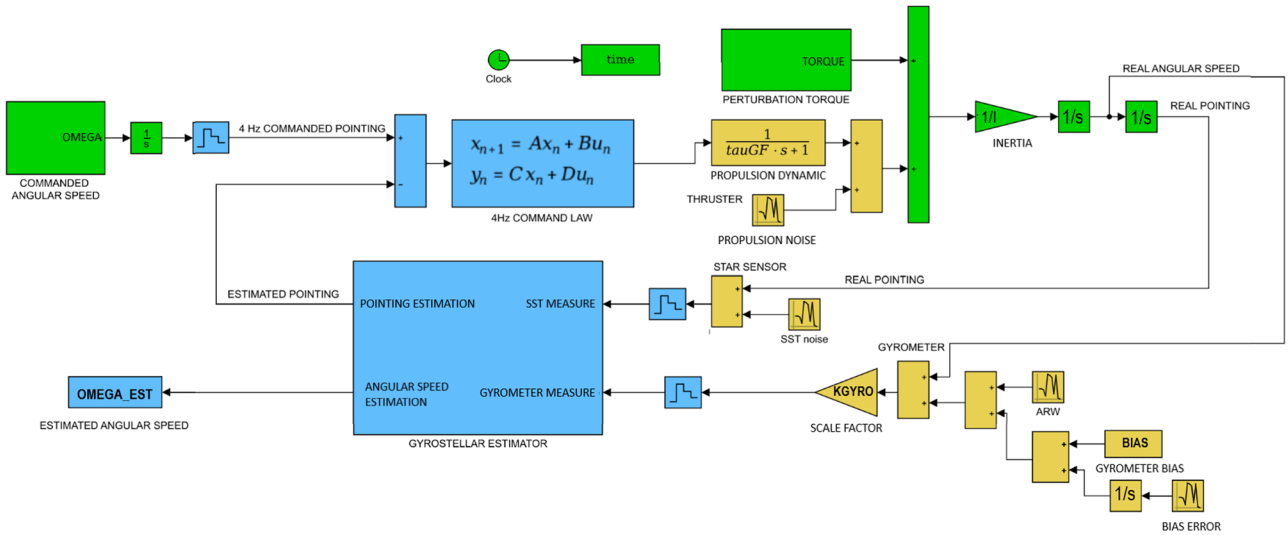

Fig. 7 Diagram of the AOCS simulator. The dynamics and perturbation torques are in green, the equipment models are in yellow and the software parts (control and estimator) are in blue.

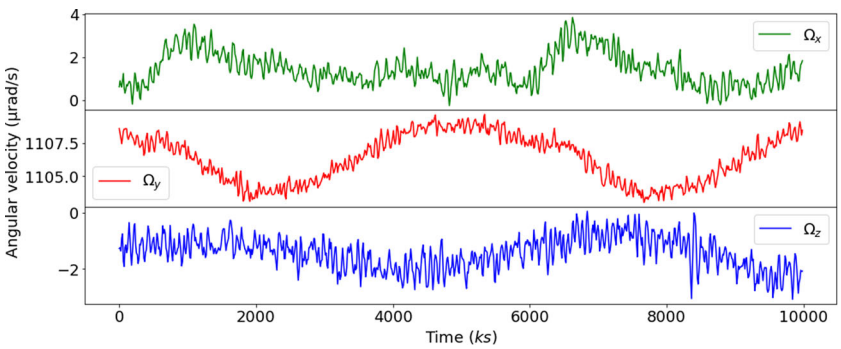

Fig. 8 Angular velocity time series of the satellite. Rotation rate around the *x*-axis (green), the *y*-axis (red) and the *z*-axis (blue).

The resulting angular velocity time series are presented in Fig. 8. Residual angular velocity fluctuations are at the μrad/s level. A periodic variation of the commanded angular velocity around *y*-axis with an amplitude of about 3 μrad/s was added to take into account the orbit eccentricity.

Reporting summary

Further information on research design is available in the Nature Research Reporting Summary linked to this article.

DATA AVAILABILITY

The datasets used and/or analyzed during the current study available from the corresponding author on reasonable request.

Received: 13 December 2022; Accepted: 15 June 2023;
Published online: 10 July 2023

REFERENCES

1. Geiger, R., Landragin, A., Merlet, S. & Pereira Dos Santos, F. High-accuracy inertial measurements with cold-atom sensors. *AVS Quantum Sci.* **2**, 024702 (2020).
2. Müntinga, H. et al. Interferometry with bose-einstein condensates in microgravity. *Phys. Rev. Lett.* **110** https://doi.org/10.1103/PhysRevLett.110.093602 (2013).
3. Frye, K. et al. The bose-einstein condensate and cold atom laboratory. *EPJ Quantum Technol.* **8**, 1 (2021).
4. Kaltenbaek, R. et al. Quantum technologies in space. *Exp. Astron.* **51**, 1677–1694 (2021).
5. Alonso, I. et al. Cold atoms in space: community workshop summary and proposed road-map. *EPJ Quantum Technol.* **9**, 1–55 (2022).
6. Chiow, S. W., Williams, J. & Yu, N. Laser-ranging long-baseline differential atom interferometers for space. *Phys. Rev. A: At. Mol. Opt. Phys.* **92**, 063613 (2015).
7. Carraz, O., Siemes, C., Massotti, L., Haagmans, R. & Silvestrin, P. A spaceborne gravity gradiometer concept based on cold atom interferometers for measuring earth's gravity field. *Microgr. Sci. Technol.* **26**, 139–145 (2014).
8. Lévèque, T. et al. Gravity field mapping using laser-coupled quantum accelerometers in space. *J. Geodesy* **95**, 1–19 (2021).
9. Trimeche, A. et al. Concept study and preliminary design of a cold atom interferometer for space gravity gradiometry. *Classical Quantum Gravity* **36**, 215004 (2019).
10. Migliaccio, F. et al. Mocass: A satellite mission concept using cold atom interferometry for measuring the earth gravity field. *Surv. Geophys.* **40**, 1029–1053 (2019).
11. Zahzam, N. et al. Hybrid electrostatic—atomic accelerometer for future space gravity missions. *Remote Sensing* **14**, 3273 (2022).
12. Aguilera, D. N. et al. Ste-quest-test of the universality of free fall using cold atom interferometry. *Classical Quantum Gravity* **31**, 115010 (2014).
13. Bassi, A. et al. A way forward for fundamental physics in space. *npj Microgravity* **8**, 1–15 (2022).
14. Dimopoulos, S., Graham, P. W., Hogan, J. M., Kasevich, M. A. & Rajendran, S. Atomic gravitational wave interferometric sensor. *Phys. Rev. D* **78**, 122002 (2008).
15. Hogan, J. M. et al. An atomic gravitational wave interferometric sensor in low earth orbit (agis-leo). *General Relativity Gravitation* **43**, 1953–2009 (2011).
16. Lévèque, T. et al. Carioqa: Definition of a quantum pathfinder mission. Preprint at https://arxiv.org/abs/2211.01215 (2022).
17. Lan, S. Y., Kuan, P. C., Estey, B., Haslinger, P. & Müller, H. Influence of the coriolis force in atom interferometry. *Phys. Rev. Lett.* **108**, 090402 (2012).
18. Peters, A., Chung, K. Y. & Chu, S. Measurement of gravitational acceleration by dropping atoms. *Nature* **400**, 849–852 (1999).
19. Guirk, J. M. M., Foster, G. T., Fixler, J. B., Snadden, M. J. & Kasevich, M. A. Sensitive absolute-gravity gradiometry using atom interferometry. *Phys. Rev. A* **65**, 033608 (2002).
20. Louchet-Chauvet, A. et al. The influence of transverse motion within an atomic gravimeter. *New J. Phys.* **13**, 065025 (2011).
21. Lévèque, T., Gauguet, A., Michaud, F., Pereira Dos Santos, F. & Landragin, A. Enhancing the area of a raman atom interferometer using a versatile double-diffraction technique. *Phys. Rev. Lett.* **103**, 080405 (2009).
22. Freier, C. et al. Mobile quantum gravity sensor with unprecedented stability. *J. Phys.: Conf. Ser.* **723**, 012050 (2016).
23. Dickerson, S. M., Hogan, J. M., Sugarbaker, A., Johnson, D. M. & Kasevich, M. A. Multiaxis inertial sensing with long-time point source atom interferometry. *Phys. Rev. Lett.* **111**, 083001 (2013).
24. Caldani, R., Weng, K. X., Merlet, S. & Pereira Dos Santos, F. Simultaneous accurate determination of both gravity and its vertical gradient. *Phys. Rev. A* **99**, 33601 (2019).
25. Deppner, C. et al. Collective-mode enhanced matter-wave optics. *Phys. Rev. Lett.* **127**, 100401 (2021).
26. Cheinet, P. et al. Measurement of the sensitivity function in a time-domain atomic interferometer. *IEEE Trans. Instrum. Meas.* **57**, 1141–1148 (2008).
27. Touboul, P. & Rodrigues, M. The MICROSCOPE space mission. *Classical Quantum Gravity* **18**, 2487–2498 (2001).
28. Ghezal, M., Polle, B., Rabejac, C. & Montel, J. Gyro Stellar Attitude Determination. *Conference: Guidance Navigation Control Syst. ADS* **606**, 22 (2006).

ACKNOWLEDGEMENTS

The authors thank Peter Wolf and Robin Corgier for stimulating discussions. This work benefited from a government grant managed by the Agence Nationale de la Recherche under the Plan France 2030 with the reference "ANR-22-PETQ-0005".

AUTHOR CONTRIBUTIONS

Q.B. and F.P. did the calculations, J.G.B., V.C., and L.A.S. conducted the experiment, S.M. designed the experiment, J.L., C.F., and T.L. conducted the attitude control simulation and Q.B. analyzed the results. All authors reviewed the manuscript.

COMPETING INTERESTS

The authors declare no competing interests.

ADDITIONAL INFORMATION

Supplementary information The online version contains supplementary material available at https://doi.org/10.1038/s41526-023-00297-w.

Correspondence and requests for materials should be addressed to Quentin Beaufils.

Reprints and permission information is available at http://www.nature.com/reprints

Publisher's note Springer Nature remains neutral with regard to jurisdictional claims in published maps and institutional affiliations.

Open Access This article is licensed under a Creative Commons Attribution 4.0 International License, which permits use, sharing, adaptation, distribution and reproduction in any medium or format, as long as you give appropriate credit to the original author(s) and the source, provide a link to the Creative Commons license, and indicate if changes were made. The images or other third party material in this article are included in the article's Creative Commons license, unless indicated otherwise in a credit line to the material. If material is not included in the article's Creative Commons license and your intended use is not permitted by statutory regulation or exceeds the permitted use, you will need to obtain permission directly from the copyright holder. To view a copy of this license, visit http://creativecommons.org/licenses/by/4.0/.

© The Author(s) 2023